Chemistry of Metals and Alloys

Chem. Met. Alloys 16 (2023) 43-51
Ivan Franko National University of Lviv
http://publications.lnu.edu.ua/chemetal

The Cu_2S–GeS_2–P_2S_5 system

Orysia BEREZNYUK[1], Oleksandr SMITIUKH[1], Lyubomyr GULAY[1], Iryna PETRUS'[1], Lyudmyla PISKACH[1]*

[1] *Department of Inorganic and Physical Chemistry, Lesya Ukrainka Volyn National University, Voli Ave. 13, 43025 Lutsk, Ukraine*
* *Corresponding author. Tel.:* +380509111265*; e-mail: piskach.lyudmyla@vnu.edu.ua*

Received October 18, 2023; accepted December 19, 2023
https://doi.org/10.30970/cma16.0433

The isothermal section of the Cu_2S–GeS_2–P_2S_5 system at 500 K was investigated. The phase interactions in the system are characterized by the formation of considerable solid solution ranges of Cu_2S, Cu_7PS_6, Cu_3PS_4, Cu_8GeS_6, and Cu_2GeS_3. According to the results of differential thermal analysis and X-ray diffraction, the phase diagrams of the Cu_8GeS_6–Cu_7PS_6 and Cu_2GeS_3–Cu_3PS_4 sections at 300 K feature extended solid solution ranges. In the former section, they range up to 30 mol.% based on the LT-Cu_7PS_6 modification (SG $P2_13$), and 10–32 mol.% Cu_7PS_6 between the HT modifications of the argyrodite compounds (SG F-43m). The solid solution range of Cu_3PS_4 (SG $Pmn2_1$) extends up to 45 mol.%, and that of Cu_2GeS_3 (SG Cc) slightly over 10 mol.%. However, the systems are not quasi-binary in the entire temperature range due to the peritectic character of melting of Cu_8GeS_6 and Cu_3PS_4. The phase diagram of the quasi-binary system Cu_2S–GeS_2 was re-investigated by differential thermal analysis and X-ray diffraction. The incongruent nature of the melting of Cu_4GeS_4 at 1209 K was established.

Solid solution / Crystal structure / Phase diagram / Isothermal section / X-ray diffraction

Introduction

Ternary copper(I) germanium sulfides have received considerable attention over the years due to the fact that they exhibit interesting properties that make them promising high-performance functional materials. In particular, the compounds Cu_8GeS_6 and Cu_2GeS_3, which form in the system Cu_2S–GeS_2, and their alloys have valuable thermoelectric, photoelectric, optical, and other properties [1-6]. Cu_4GeS_4 is a candidate for the development of new highly efficient functional materials [6,7]. Materials with ion-electron conductivity based on superionic semiconductors such as Cu_7PS_6 are also of particular interest [8]. These compounds with argyrodite structure have high cationic conductivity in the solid state and important physico-chemical properties. They are used as photoelectrode materials, electrochemical converters of solar energy, ionizers, *etc.* [8-10]. Glasses based on germanium(IV) sulfide are used for high-speed data transmission by optical waveguides and integrated circuits, as ceramics for thermal information display, and components of lithium energy-intensive batteries [11]. Phosphorus(V) sulfide can also act as a glass-forming agent and is the starting material for a number of thiophosphate compounds [12,13]. It is worth noting that significant solid solutions based on these sulfides may exist in the system.

The compound Cu_2S forms in the binary system Cu–S, melts congruently at 1403 K, and has three polymorphous modifications, orthorhombic (α-Cu_2S is stable to 376.5 K), hexagonal (α'-Cu_2S is stable in the range 376.5-708 K), and cubic (α"-Cu_2S, 708-1403 K) [14]. GeS_2 melts congruently at 1123 K [15] and crystallizes in two modifications, both monoclinic, SG Pc (LT-GeS_2) [16] and SG $P2_1/c$ [17]. Phosphorus(V) sulfide forms congruently (various authors give virtually identical melting points within 553-558 K [12,18]), and crystallizes in the triclinic symmetry, SG P-1 [13].

The quasi-binary section Cu_2S–GeS_2 has often been investigated, with much inconsistency. The existence of Cu_8GeS_6 (cuprodite mineral analog) and Cu_2GeS_3 is always confirmed, but the character of the crystallization is different [19-21]. Recent studies of the phase equilibria [21] indicate that Cu_8GeS_6 melts incongruently at 1253 K, and Cu_2GeS_3 melts congruently at 1253 K, but the existence of Cu_4GeS_4 [6,7] and $Cu_2Ge_2S_5$ [1,6,7] was not confirmed. At 328 K a phase transition was registered for Cu_8GeS_6 [20] (LTM-Cu_8GeS_6 (SG $Pmn2_1$) ↔ HTM-Cu_8GeS_6 (SG F-43m)). Crystallographic details of the compounds identified in the Cu_2S–GeS_2 system are presented in Table 1.

Literature sources [25,26] are controversial regarding the character of the physico-chemical

interactions in the Cu_2S–P_4S_{10} system, specifically on the melting nature of Cu_7PS_6 and on the existence of $CuPS_3$. Andrae and Blachnik [25] report three compounds in the system, Cu_7PS_6 (congruent melting at 1327 K, polymorphous transformation at 515 K (LTM-Cu_7PS_6 (SG $P2_13$) ↔ HTM-Cu_7PS_6 (SG F-43m)), Cu_3PS_4 (melts incongruently at 1237 K), and $CuPS_3$ (melts incongruently at 707 K). However, Galagovets and Potorii [26] assert incongruent melting for Cu_7PS_6 at 1300 K and do not confirm the existence of the compound $CuPS_3$. Crystallographic details of the compounds reported in the Cu_2S–P_3S_5 system are listed in Table 2.

We have previously investigated the Cu_8GeS_6–Cu_7PS_6 section formed by the copper-containing argyrodites in this quasi-ternary system [29]. The section at 300 K shows significant ranges of solid solutions, up to 30 mol.% based on LT-Cu_7PS_6 (β), from 10 to 32 mol.% Cu_7PS_6 based on HT-Cu_8GeS_6 and Cu_7PS_6 (δ), which can be expressed by the formula $Cu_{8-x}Ge_{1-x}P_xS_6$ (x=0-1). Solid solubility in LT-Cu_8GeS_6 (σ) does not exceed 5 mol.%. The section is not quasi-binary in the entire temperature range due to peritectic melting of Cu_8GeS_6. This leads to the crystallization of solid solutions of HT-Cu_2S (α′′) up to 70 mol.% Cu_7PS_6. The range above 70 mol.% Cu_7PS_6 features primary crystallization of the $Cu_{8-x}Ge_{1-x}P_xS_6$ solid solution with the cubic structure (SG F-43m). Due to the formation of this LT solid solution, the temperatures of polymorphous transformations of both ternary compounds are significantly reduced (Fig. 1).

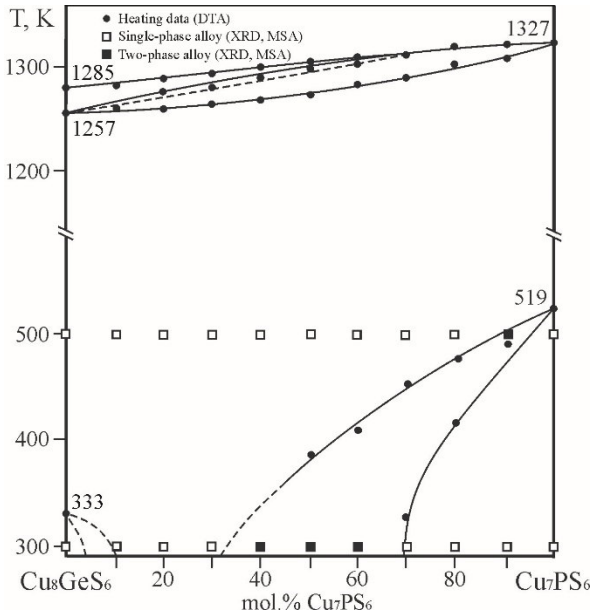

Fig. 1 The Cu_8GeS_6–Cu_7PS_6 phase diagram [29].

Experimental part

For the synthesis of the samples, chemical elements of high purity were used: copper (99.99 wt.%), germanium (monocrystalline, 99.999 wt.%), phosphorous red (99.98 wt.%), sulfur (99.99 wt.%). The weighing of the calculated amounts of source materials was performed on VLA-200 scales with an accuracy of ±0.00005 g based on 1.5 g charges in quartz tubes with a diameter of 8-10 mm and a wall thickness of 1.5 mm. The tubes were evacuated to a residual pressure of $1.33 \cdot 10^{-2}$ Pa. The synthesis was carried out by the direct single-temperature method in an automatic muffle furnace MP-60 with a program temperature controller PR-04. Initially, the samples were heated to 670 K at a rate of 20 K/h, and annealed at this temperature for 48 h.

Table 1 Crystallographic details of the identified compounds of the Cu_2S–GeS_2 system.

Compound		LTM-Cu_8GeS_6	HTM-Cu_8GeS_6	Cu_4GeS_4	Cu_2GeS_3
SG		$Pmn2_1$	F-43m	$P2_1/c$	Cc
System		*orthorhombic*	*cubic*	*monoclinic*	*monoclinic*
Pearson code		*oP*30	*cF*60	*mP*72	*mS*24
Lattice parameters, nm	a	0.70445	0.99567	0.9790	0.6449
	b	0.69661	...	1.3205	1.1319
	c	0.98699	...	0.9942	0.6428
Angle		...	...	β=100.90°	β=108.37°
Ref.		[22]	[23]	[7]	[24]

Table 2 The crystallographic details of the identified compounds of the Cu_2S–P_2S_5 system.

Compounds		LTM-Cu_7PS_6	HTM- Cu_7PS_6	Cu_3PS_4
SG		$P2_13$	F-43m	$Pmn2_1$
Symmetry		*cubic*	*cubic*	*orthorhombic*
Pearson code		*cP*56	*cF*56	*oP*16
Lattice parameters, nm	a	0.9673(1)	0.971(2)	0.72817
	b	...	...	0.63387
	c	...	...	0.60746
Ref.		[27]	[27]	[28]

They were then heated to 870 K at a rate of 6 K/h, held for 48 h, and further heated to 1170 K at a rate of 6 K/h. After holding for 10 h at the maximum temperature, they were gradually cooled (10 K/h) to 500 K. At this temperature, the samples were annealed for 240 h, then the furnace was switched off.

All the samples were analyzed using a range of physicochemical methods (XRD, DTA). Powder X-ray diffraction patterns were obtained using a DRON 4-13 diffractometer (Cu Kα radiation) with the following parameters: angle range $10° \le 2\theta \le 70°$, step 0.05°, exposure time at each point 4 s. The investigation of the crystal structure of the solid solutions was performed by the powder method based on experimental data obtained using a DRON 4-13 diffractometer (Cu *K*α radiation, angle range $10° \le 2\theta \le 100°$, step size 0.05°, exposure time at each point 20 s). All calculations were performed using the WinCSD program [30].

DTA was performed on an installation consisting of a furnace with regulated heating "Thermosdent-03" from NTF Progret, a block of signal amplification of the thermocouple. Pre-burned Al_2O_3 for 10 h at 1170 K was used as standard. The temperature sensor was a combined Pt/Pt-Rh thermocouple. The furnace was uniformly heated using program control at a rate of 10 K/min, and cooled in an inertial mode. The maximum heating temperature was 1300 K. The accuracy of temperature effect registration was ±5 K.

Results and discussion

The Cu_2S–GeS_2–P_2S_5 system. Sixty samples were synthesized and investigated in the Cu_2S–GeS_2–P_2S_5 system. Five ternary compounds, Cu_8GeS_6, Cu_2GeS_3, Cu_4GeS_4, Cu_7PS_6, and Cu_3PS_4, exist in this system. The compounds $Cu_2Ge_2S_5$ and $CuPS_3$ were not found at 500 K. The sample with composition '$Cu_2Ge_2S_5$' was two-phase: Cu_2GeS_3 (SG *Imm*2) + GeS_2 (SG $P2_1/c$).

The Cu_2S–GeS_2 section. Two compounds, at 25 and 50 mol.% GeS_2, exist in the section. The Cu_4GeS_4 phase was not found in [21], whereas its crystal structure was reported by others [7]. We concluded that their experiments differed in the conditions and decided to re-investigate this section. The phase diagram in the 0-70 mol.% GeS_2 range is presented here (Fig. 2*a*). The existence of the Cu_4GeS_4 compound melting incongruently L + δ'-Cu_8GeS_6 ↔ Cu_4GeS_4 at 1209 K was confirmed (Fig. 2*b*). The homogeneity regions of Cu_2S, Cu_8GeS_6, and Cu_2GeS_3 were determined.

The Cu_2GeS_3–Cu_3PS_4 section. The Cu_2GeS_3–Cu_3PS_4 section is a two-phase equilibrium in the solid state (Fig. 3), with substantial solid solution ranges of the end compounds at 500 K. All the samples with 50-100 mol.% Cu_3PS_4 are single-phase and form the $Cu_{3-(x/3)}Ge_{4/3x}P_{1-x}S_4$ solid solution. The lattice parameters gradually increase with decreasing Cu_3PS_4 content (Fig. 4).

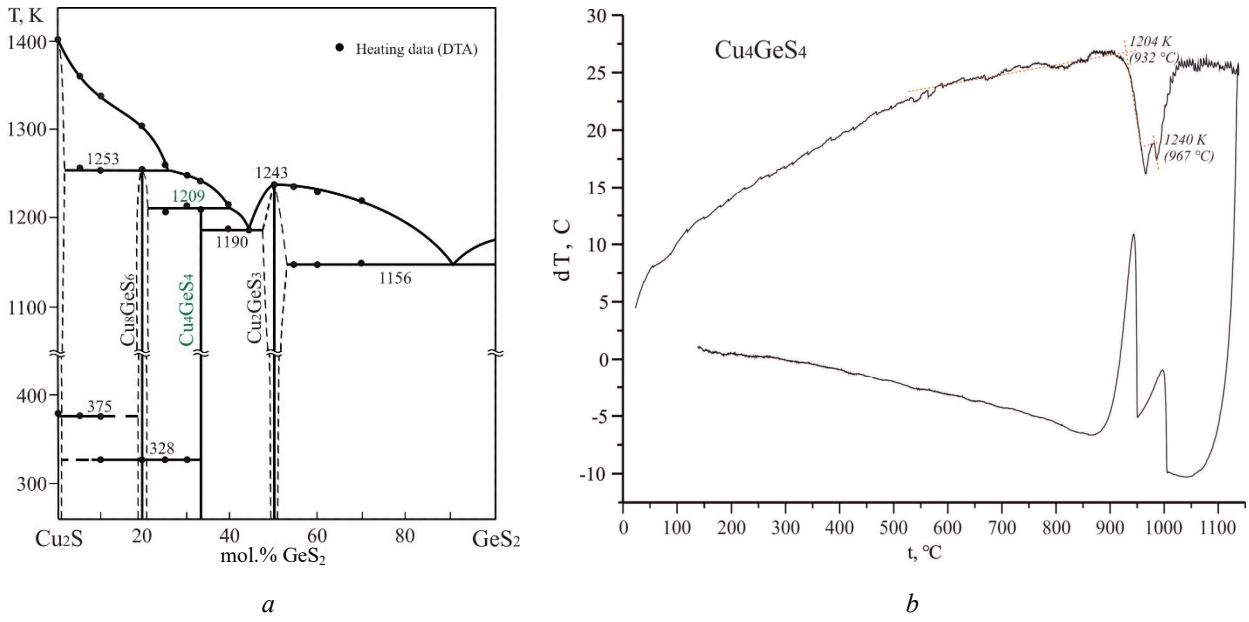

Fig. 2 *a*) The Cu_2S–GeS_2 phase diagram [this work]; *b*) the DTA curve for incongruent melting Cu_4GeS_4 compound.

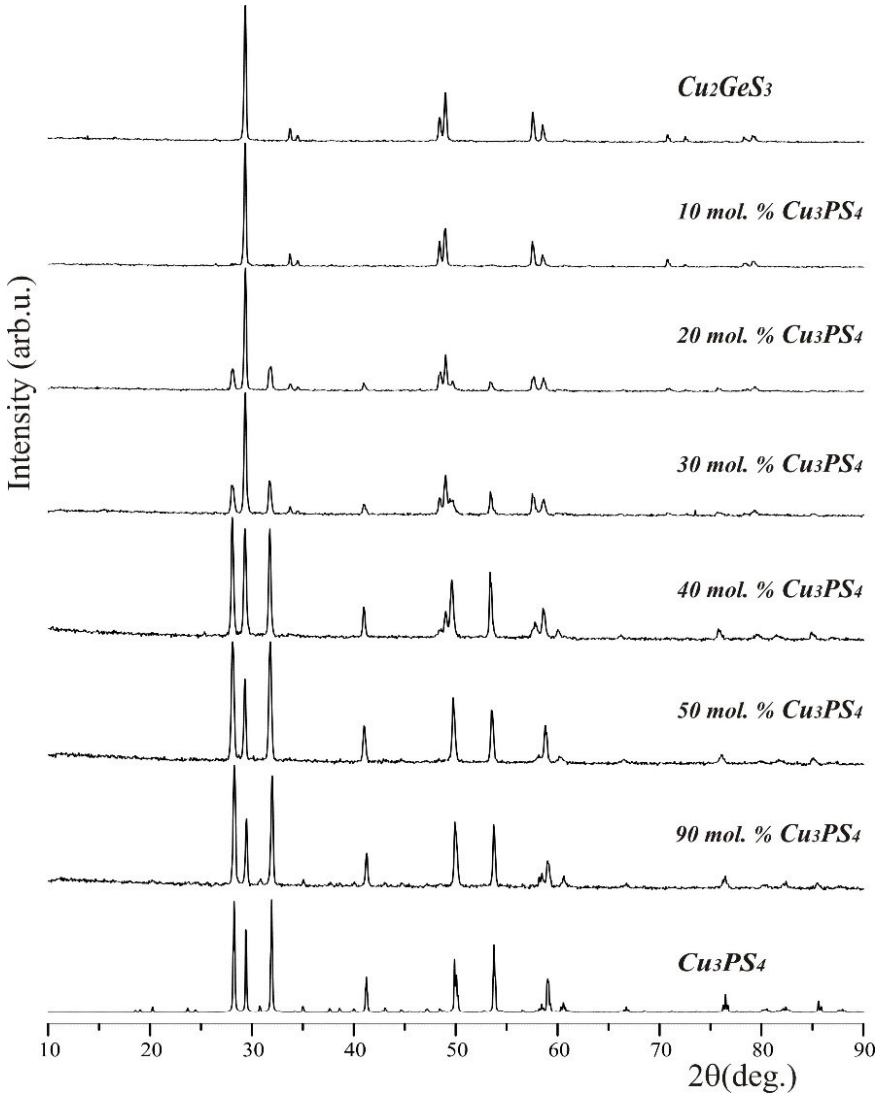

Fig. 3 Diffraction patterns of the alloys of the Cu_2GeS_3–Cu_3PS_4 section.

Table 3 Lattice parameters of the $Cu_3P_{1-x}Ge_xS_4$ solid solution.

Composition, mol.%		SG	Lattice period, nm			V, nm^3
Cu_2GeS_3	Cu_3PS_4		*a*	*b*	*c*	
10	90	$Pmn2_1$	0.7283(8)	0.6336(7)	0.6075(5)	0.28038(8)
20	80	$Pmn2_1$	0.7296(2)	0.6350(2)	0.6086(9)	0.2820(2)
30	70	$Pmn2_1$	0.7302(10)	0.6352(7)	0.6090(5)	0.28238(9)
40	60	$Pmn2_1$	0.7304(7)	0.6356(6)	0.6093(4)	0.28289(7)
50	50	$Pmn2_1$	0.7320(2)	0.6369(2)	0.6100(9)	0.2844(2)
60	40	$Pmn2_1$	0.7321(2)	0.6369(3)	0.6101(2)	0.2845(2)

The ε-solid solution range of Cu_2GeS_3 extends up to 10 mol.%, and the γ-solid solution of Cu_3PS_4 up to 50 mol.%. The substitution of Ge atoms for P atoms in the γ-solid solution leads to a gradual increase of the lattice parameters (Fig. 4, Table 3). It may also affect the electrical and optical properties of the compound, as the electronic structure and band gap can be sensitive to changes in the atomic composition and arrangement. The ε-solid solution range of Cu_2GeS_3, on the other hand, is relatively narrow, indicating that the incorporation of foreign atoms into this compound is more limited. Understanding the solid solution ranges and their dependence on composition and temperature is important for designing and optimizing materials with specific properties for various applications, such as in electronic devices, solar cells, and catalysis.

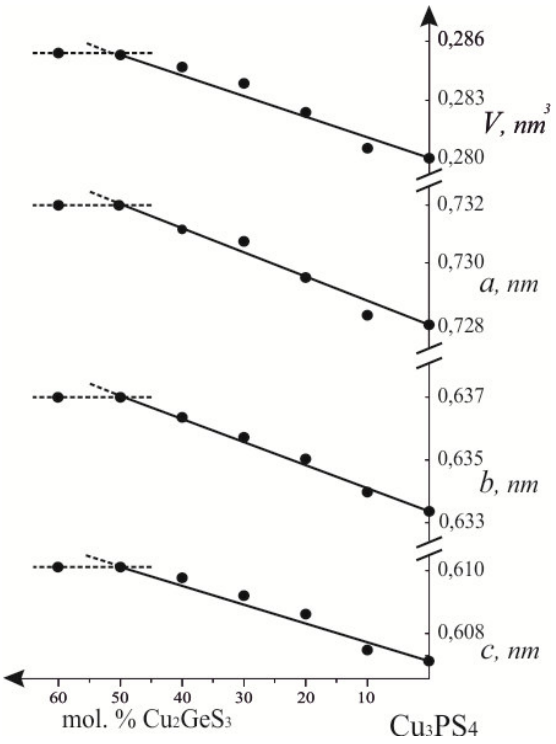

Fig. 4 Change of lattice parameters in the Cu_2GeS_3–Cu_3PS_4 section.

The crystal structure of the $Cu_{3-(x/3)}Ge_{4/3x}P_{1-x}S_4$ solid solution was refined for $x = 1/3$. The peaks of the X-ray powder diffraction pattern were indexed based on an orthorhombic unit cell with the lattice parameters listed in Table 4. The structure of Cu_3PS_4 (SG $Pmn2_1$) was used as a starting model for the structure refinement. The substitution of Ge atoms both for P and for Cu atoms in the position Cu1 was observed. The values of the occupancy factors for Cu1 and P1 were fixed at 0.889 Cu + 0.111 Ge and 0.667 P + 0.333 Ge to satisfy charge balance requirements. The calculated composition agrees well the composition of the sample. The conditions of the X-ray experiment and the crystallographic parameters are presented in Table 4. Atomic coordinates and isotropic displacement parameters for $Cu_{26/9}Ge_{4/9}P_{2/3}S_4$ are listed in Table 5. The experimental and calculated diffractograms and the corresponding difference diagram for $Cu_{26/9}Ge_{4/9}P_{2/3}S_4$ are shown in Fig. 5. The crystal structure consists of S_4 tetrahedrons around the metallic elements (Fig. 6). The mixtures [CuGe] and [PGe] are located in Wyckoff position 2*a*.

According to DTA results, the Cu_2GeS_3–Cu_3PS_4 section is not quasi-binary in the entire temperature range due to the incongruent melting of Cu_3PS_4 (Fig. 7). The samples with up to 20 mol.% Cu_3PS_4 feature primary crystallization of the Cu_2GeS_3 solid solution. The solid solutions of HT-Cu_7PS_6 crystallize from 20 to 60 mol.% Cu_3PS_4, and then appears the solid solutions of Cu_3PS_4. The horizontals at 1127 and 1210 K belong to the three-phase processes in the Cu_2S–GeS_2–P_2S_5 system.

Isothermal section of the Cu_2S–GeS_2–P_2S_5 system at 500 K. The phase equilibria in the Cu_2S–GeS_2–P_2S_5 system at 500 K in the entire concentration range were investigated by XRD and DTA.

The phase interactions in the system lead to the formation of solid solution ranges of β-Cu_7PS_6, γ-Cu_3PS_4, δ-Cu_8GeS_6, and ε-Cu_2GeS_3 (Figs. 1,7,8). However, the solid solubility of the binary compounds GeS_2 and P_2S_5, and of the ternary compound Cu_4GeS_4 compounds is negligible. Wide-range solid solutions based on β-Cu_7PS_6, γ-Cu_3PS_4, δ-Cu_8GeS_6, and ε-Cu_2GeS_3 compounds are a group of materials that exhibit a range of properties due to their unique crystal structures and chemical compositions.

Table 4 Crystallographic parameters of $Cu_{26/9}Ge_{4/9}P_{2/3}S_4$.

Parameters	$Cu_{26/9}Ge_{4/9}P_{2/3}S_4$
Space group	$Pmn2_1$
a, nm	0.73044(7)
b, nm	0.63562(6)
c, nm	0.60931(4)
Cell volume, nm³	0.28289(7)
Number of atoms in the cell	16
Density (calculated), g/cm³	4.281(1)
Absorption coefficient, 1/cm	294.69
Radiation and wavelength, nm	Cu*K*α; 0.154158
Diffractometer	DRON 4-13
Mode of refinement	Full profile
Program	CSD
Number of atom sites	6
Reflections used in refinement	2
2θ and $\sin\theta/\lambda$ (max)	90.05; 0.459
R_I	0.0710
R_P	0.2447

Table 5 Isotropic coordinates and displacement parameters of atoms in the $Cu_{26/9}Ge_{4/9}P_{2/3}S_4$ structure.

Atoms	Wyckoff position	*x/a*	*y/b*	*z/c*	$B_{iso}\times10^2$, nm^2
Cu1*	2*a*	0	0.6543(15)	0.100(2)	1.5(3)
Cu2	4*b*	0.7458(12)	0.1747(11)	0.0933(12)	1.79(14)
P1*	2*a*	0	0.319(2)	0.608(3)	1.4(3)
S1	2*a*	0	0.312(4)	0.256(2)	1.3(5)
S2	2*a*	0	0.636(3)	0.720(3)	1.6(4)
S3	4*b*	0.728(2)	0.831(3)	0.2077(13)	1.3(3)

* occupation Cu1 (0.889 Cu + 0.111 Ge); P1 (0.667 P + 0.333 Ge)

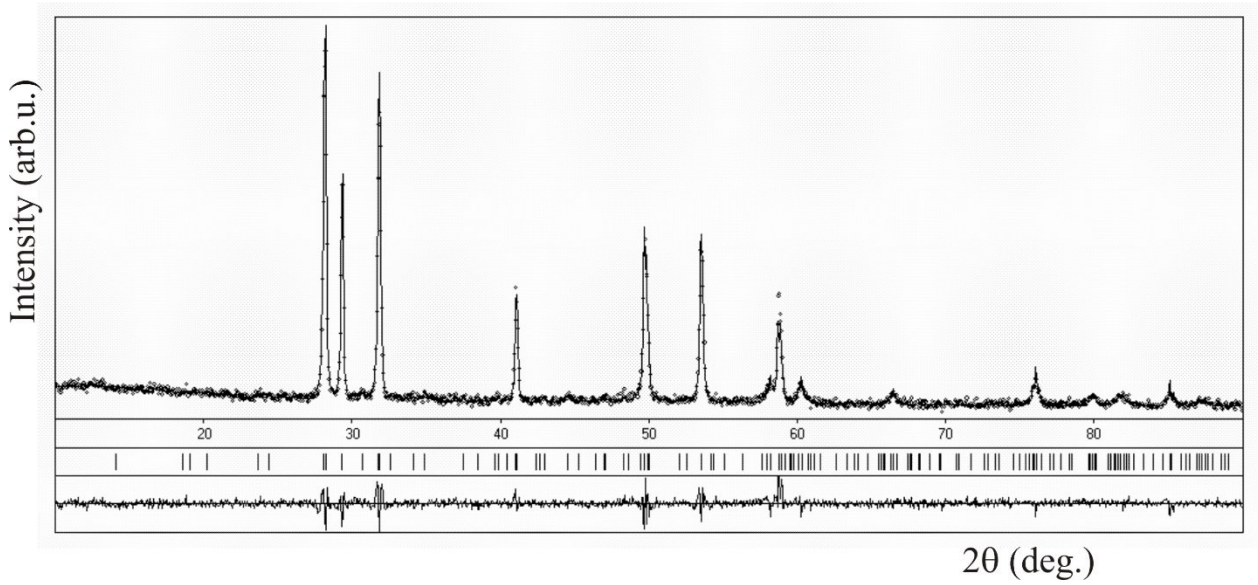

Fig. 5 Experimental and theoretical diffractograms of $Cu_{26/9}Ge_{4/9}P_{2/3}S_4$.

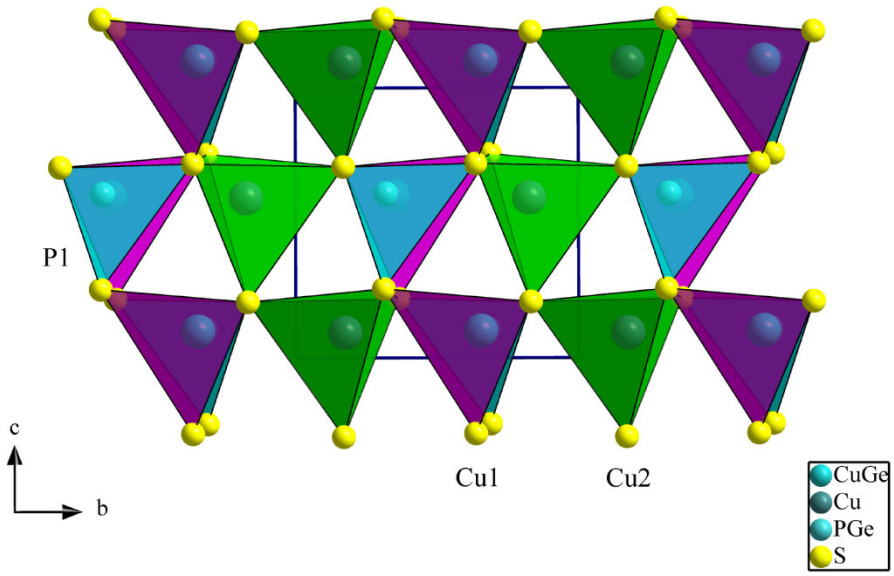

Fig. 6 Coordination polyhedrons of the Cu, P, and Ge atoms in the structure of $Cu_{26/9}Ge_{4/9}P_{2/3}S_4$.

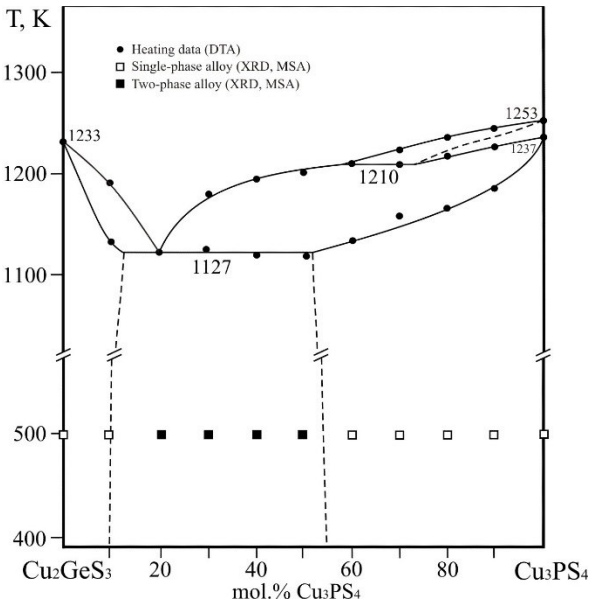

Fig. 7 The phase diagram of Cu_3PS_4–Cu_2GeS_3.

These materials are composed of copper, phosphorus, sulfur, and germanium, which are combined in different ratios to form solid solutions. The compound β-Cu_7PS_6 exhibits high ionic conductivity and is used as an electrolyte in batteries and fuel cells. The compound γ-Cu_3PS_4 exhibits high thermoelectric performance and is used in thermoelectric generators. δ-Cu_8GeS_6 exhibits high mechanical strength and is used in structural applications. ε-Cu_2GeS_3 exhibits high optical transparency and is used in optical devices. The solid solutions based on the compounds may have potential applications in various fields such as energy storage, structural materials, and optoelectronics.

According to the phase analysis of the sample at the intersection of the possible equilibria Cu_2GeS_3–Cu_7PS_6 and Cu_4GeS_4–Cu_3PS_4 (69 mol.% Cu_2S / 25 mol.% GeS_2 / 6 mol.% P_2S_5), it contains Cu_7PS_6 + Cu_2GeS_3. This proves the existence of the region β–ε and contradicts the existence of binary equilibrium between Cu_3PS_4 and Cu_4GeS_4. The isothermal section of the Cu_2S–GeS_2–P_2S_5 system at 500 K is presented in Fig. 8.

The system features 8 single-phase regions (α', GeS_2, P_2S_5, β, γ, δ', Cu_4GeS_4, and ε) that form 13 two-phase regions (α' + β, β + γ, γ + P_2S_5, α' + δ, δ + Cu_4GeS_4, Cu_4GeS_4 + ε, ε + GeS_2, GeS_2 + P_2S_5, β + δ, β + Cu_4GeS_4, β + ε, γ + ε, γ + GeS_2), and 6 three-phase regions: α' + β + δ, β + δ + Cu_4GeS_4, β + Cu_4GeS_4 + ε, γ + β + ε, γ + ε + GeS_2, P_2S_5 + γ + GeS_2.

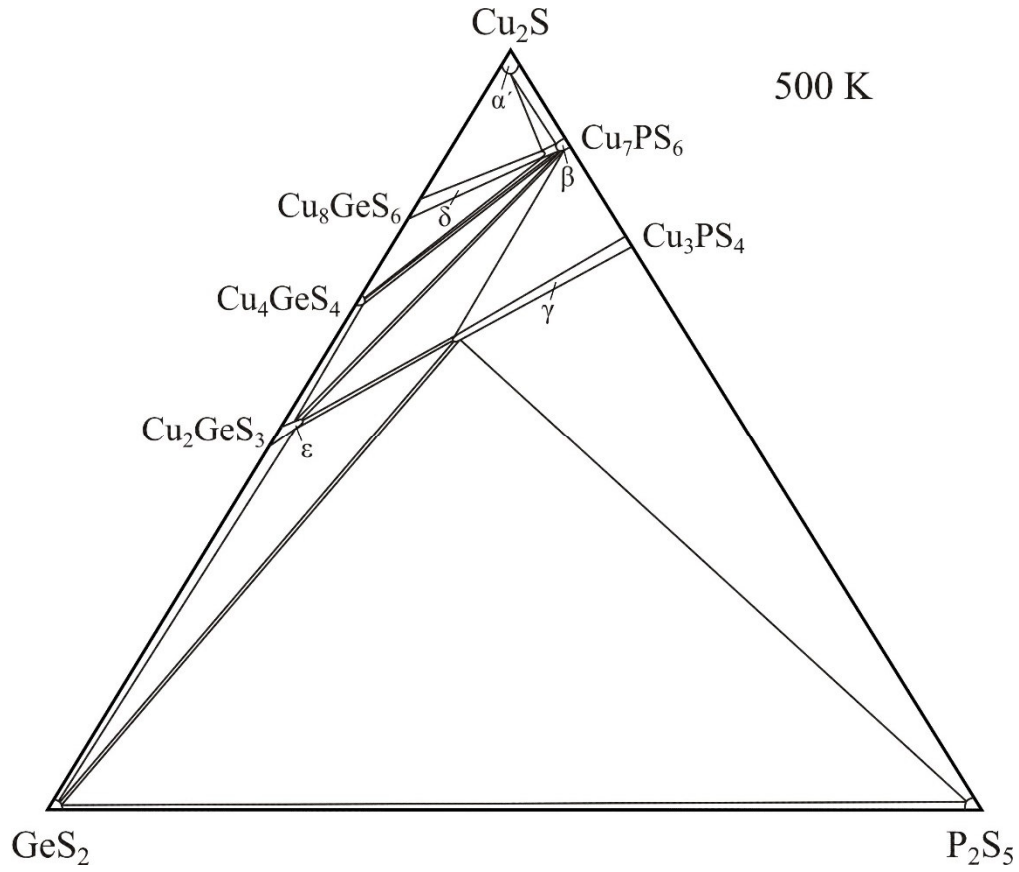

Fig. 8 Isothermal section of the Cu_2S–GeS_2–P_2S_5 system at 500 K.

Conclusions

The interaction of copper-containing phases in the Cu_2S–GeS_2–P_2S_5 system was investigated from room temperature to the melting points. The existence of the '$Cu_2Ge_2S_5$' compound was not confirmed. The presented Cu_8GeS_6–Cu_7PS_6 phase diagram is important for materials science because it contains information about the section where the Cu_8GeS_6 and Cu_7PS_6 phases coexist, as well as the conditions for their formation and stability. This information is crucial for the development of new materials with specific properties, such as high conductivity, thermal stability, and resistance to corrosion. Additionally, the phase diagram provides insights into the mechanisms of crystal growth and phase transitions, which are essential for understanding the behavior of materials under different conditions. The quasi-ternary system exhibits a considerable $Cu_{3-(x/3)}Ge_{4/3x}P_{1-x}S_4$ solid solution along the Cu_2GeS_3–Cu_3PS_4 section extending inside the concentration triangle. It is important to understand the composition and properties of this solid solution, as it can potentially exhibit unique properties that are different from those of the parent compounds. The phase diagram can help identifying the composition range where this solid solution exists, as well as the conditions under which it forms and its stability range. Furthermore, the phase diagram can also provide information on the formation of other phases, such as impurities or secondary phases that may form during synthesis or processing. This information is important for controlling the purity and quality of the final product.

References

[1] M.B. Babanly, Y.A. Yusibov, V.T. Abishev, Baku: *BSU Publisher*. 1993. 341 p.

[2] C. Coughlan, M. Ibáñez, O. Dobrozhan, A. Singh, A. Cabot, K.M. Ryan, *Chem. Rev.* 117(9) (2017) 5865-6109. https://doi.org/10.1021/acs.chemrev.6b00376

[3] V.A. Abbasova, I.J. Alverdiyev, E. Rahimoglu, R.J. Mirzoyeva, M.B. Babanly, *Azerbaijan Chem. J.* (2) (2017) 25-29.

[4] Y. Fan, G. Wang, R. Wang, B. Zhang, X. Shen, P. Jiang, X. Zhang, H. Gu, X. Lu, X. Zhou, *J. Alloys Compd.* 822(5) (2020) 153665. https://doi.org/10.1016/j.jallcom.2020.153665

[5] X. Meng, P. Gong, J. Shi, C. Li, Z. Lin, J. Yao, *Inorg. Chem*. 62(28) (2023) 10892-10896. https://pubs.acs.org/doi/10.1021/acs.inorgchem.3c01553

[6] M. Ishii, M. Onoda, X. Chen, H. Wada, K. Shibata, *Solid State Ionics* 136-137 (2000) 403-407. https://doi.org/10.1016/S0167-2738(00)00469-0

[7] X.-A. Chen, M. Onoda, H. Wada, A. Sato, H. Nozaki, R. Herbst-Irmer, *J. Solid State Chem.* 145(1) (1999) 204-211. https://doi.org/10.1006/jssc.1999.8243

[8] W.F. Kuhs, R. Nitsche, K. Scheunemann, *Mater. Res. Bull.* 14(2) (1979) 241-248. https://doi.org/10.1016/0025-5408(79)90125-9

[9] I.P. Studenyak, V.Yu. Izai, A.I. Pogodin, O.P. Kokhan, V. Sidey. M.Yu. Sabov, A. Kežionis, T. Salkus, J. Banys, *Lith. J. Phys.* 57(4) (2017) 243-251. https://doi.org/10.3952/physics.v57i4.3603

[10] B. Andriyevsky, I.E. Barchiy, I.P. Studenyak, A.I. Kashuba, M. Piasecki, *Sci. Rep.* 11(1) (2021) 19065. https://doi.org/10.1038/s41598-021-98515-6

[11] V. Mitsa, P. Holomb, G. Lovas, O. Kondrat, M. Veresh, A. Tsytrovskyi, L. Khimich, A. Chik, *Atmospheric corrosion of telecommunication optical media for chalcogenide photonics: glassy and crystalline germanium disulfide*, Breza, Uzhhorod, 2017, 126 p. (in Ukrainian).

[12] R. Blachnik, B. Gather, E. Andrae, *J. Therm. Anal. Calorim.* 37(6) (1991) 1289-1298. https://doi.org/10.1007/bf01913862

[13] R. Blachnik, J. Matthiesen, A. Müller, H. Nowottnick, H. Reuter, *Z. Kristallogr. – New Cryst. Struct*. 213 (1998) 233-234. https://doi.org/10.1524/ncrs.1998.213.14.247

[14] D.J. Chakrabarti, D.E. Laughlin, *Bull. Alloy Phase Diagr.* 4(3) (1983) 254–271. https://doi.org/10.1007/BF02868665

[15] D.I. Bletskan, *J. Ovonic Res*. 1(5) (2005) 53-60.

[16] G. Dittmar, H. Schäfer, *Acta Crystallogr. B* 31 (1975) 2060-2064. https://doi.org/10.1107/S0567740875006851

[17] G. Dittmar, H. Schäfer, *Acta Crystallogr. B* 32 (1976) 1188-1192. https://doi.org/10.1107/S0567740876004913

[18] R. Förthmann, A. Schneider, *Z. Phys. Chem.* 49 (1966) 22-37. https://doi.org/10.1524/zpch.1966.49.1_2.022

[19] M. Fiorentini Potenza, M. Elli, L. Cambi, *Atti Accad. Naz. Lincei. Cl. Sci. Fis. Mat. Natur. Rend.* 32(2) (1962) 185-191.

[20] M. Khanafer, J. Rivet, J. Flahaut, *Bull. Soc. Chim. France* 3 (1973), 859-862.

[21] I.J. Alverdiyev, *Chem. Probl.* 3(17) (2019) 423-428. https://doi.org/10.32737/2221-8688-2019-3-423-428

[22] M. Onoda, X.-A. Chen, K. Kato, A. Sato, H. Wada, *Acta Crystallogr. B* 55 (1999) 721-725. https://doi.org/10.1107/S0108768199004541

[23] L.D. Gulay, O.V. Parasyuk, Y.E. Romanyuk, *J. Alloys Compd.* 333(1-2) (2002) 109-112. https://doi.org/10.1016/S0925-8388(01)01726-1

[24] L.M. Chalbaud, G. Diaz de Delgado, J.M. Delgado, A.E. Mora, V. Sagredo, *Mater. Res. Bull.* 32(10) (1997) 1371-1376. https://doi.org/10.1016/S0025-5408(97)00115-3
[25] H. Andrae, R. Blachnik, *J. Alloys Compd.* 189(2) (1992) 209-215. https://doi.org/10.1016/0925-8388(92)90709-I
[26] I.V. Galagovets, M.V. Potorii, *Thematic Scientific and Technical Conference* (1991) 51-56. (in Ukrainian)
[27] W.F. Kuhs, M. Schulte-Kellinghaus, V. Krämer, R. Nitsche, *Z. Naturforsch. B* 32(9) (1977) 1100-1101. https://doi.org/10.1515/znb-1977-0929
[28] A. Pfitzner, S. Reiser. *Z. Kristallogr. – Cryst. Mater.* 217(2) (2002) 51-54. https://doi.org/10.1524/zkri.217.2.51.20632
[29] O.P. Berezniuk, O.V. Smitiukh, L.V. Piskach, *Probl. Chem. Sustainable Dev.* 4 (2022) 3-16. (in Ukrainian) https://doi.org/10.32782/pcsd-2022-4-1
[30] L.G. Akselrud, Yu.N. Grin', P.Yu. Zavalij, *J. Appl. Crystallogr.* 47(2) (2014) 803-805. https://doi.org/10.1107/S1600576714001058